Electronic Supplementary Material (ESI) for Soft Matter.
This journal is © The Royal Society of Chemistry 2019

Supporting Information for Dilute Solution Structure of Bottlebrush Polymers

Sarit Dutta, Matthew A. Wade, Dylan J. Walsh, Damien Guironnet, Simon A. Rogers, and Charles E. Sing*

Department of Chemical and Biomolecular Engineering, University of Illinois at Urbana-Champaign, Urbana, Illinois 61801, USA

E-mail: cesing@illinois.edu

1 Materials and characterization

1.1 Materials

Figure S1 shows GPC chromatograms for the samples synthesized.

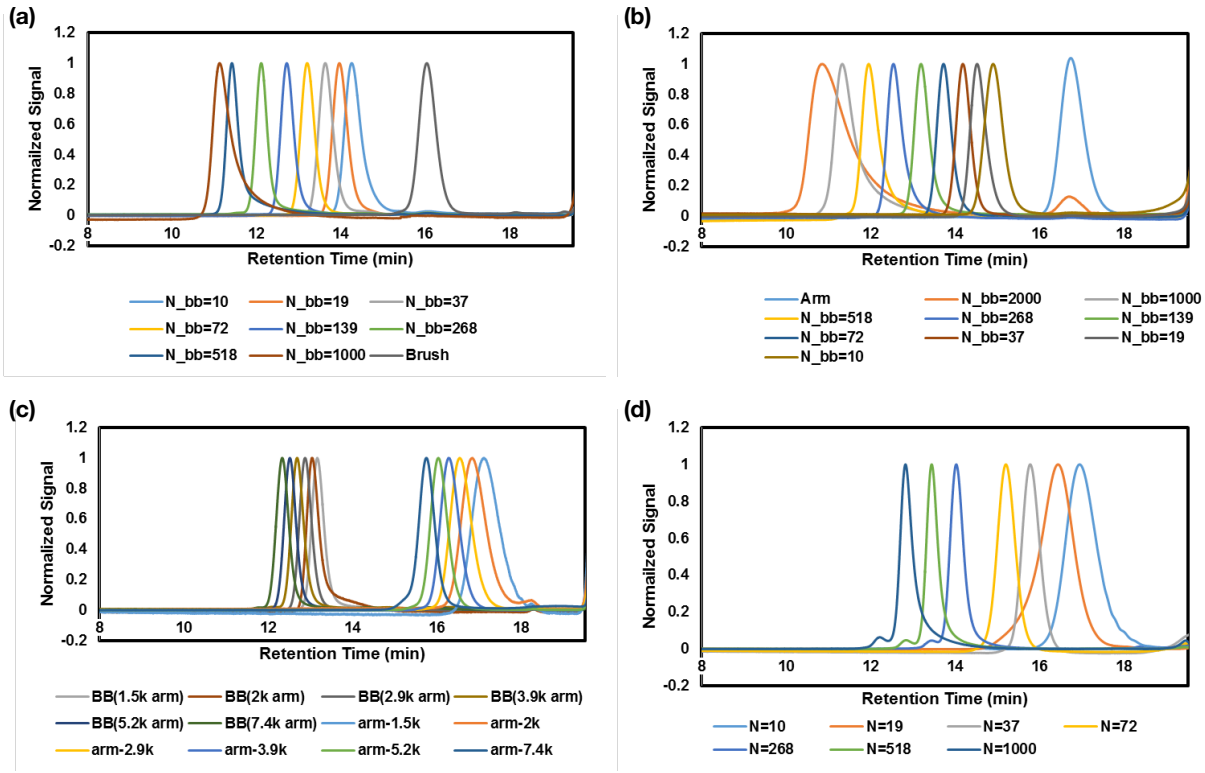

Figure S1: GPC chromatograms: (a) backbone length sweep for long side chains; (b) backbone length sweep for short side chains; (c) side chain sweep; (d) sweep for 5-norbornene-2-(methylbenzoate).

1.2 Intrinsic viscosity

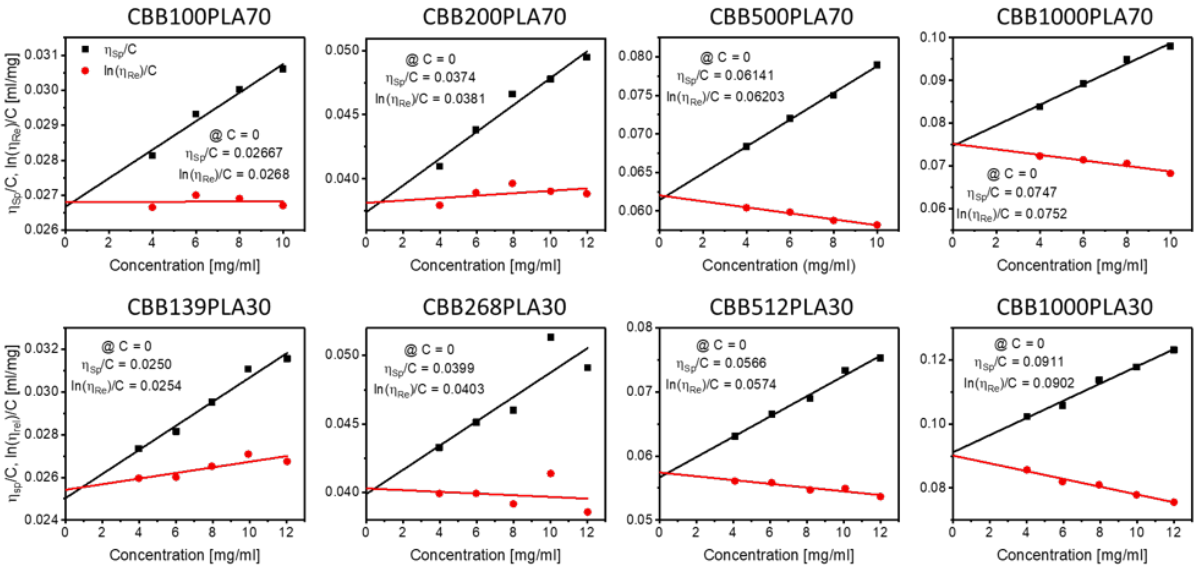

Figure S2: Viscosity measurements for an select set of bottlebrush polymers fitted using the Huggins (black) and Kraemer (red) equations. Labels above each plot correspond to the bottlebrush sample used to collect the data in each plot. The value of both fits extrapolated to zero is included in each plot.

Data collected from the two Cannon-Fenske capillary viscometers were processed and fitted according to the Huggins equation

$$\frac{\eta_{sp}}{C} = [\eta] + k_h[\eta]^2 C \tag{1}$$

and the Kraemer equation

$$\frac{\ln \eta_{rel}}{C} = [\eta] + k_k[\eta]^2 C. \tag{2}$$

In eq (1) and eq (2), $[\eta]$, η_{sp}, and η_{rel} are the intrinsic, specific, and relative viscosities of the sample, respectively; k_h and k_k are the fitting parameters for the Huggins and Kraemer equations, respectively; C is the concentration of the sample. Fits calculated using these two equations were extrapolated to zero concentration to determine the intrinsic viscosity (see Figure S2 for representative fits). Additional viscosity data can be provided upon request.

1.3 Hydrodynamic radius

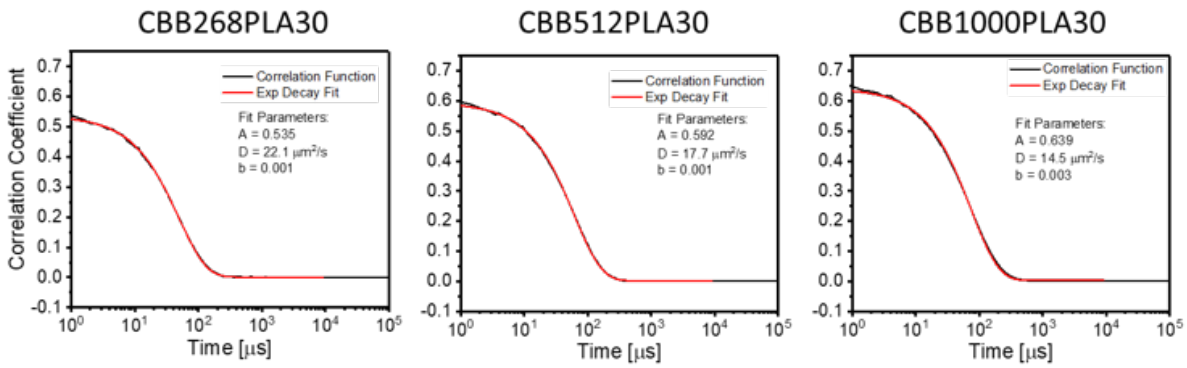

Figure S3: Autocorrelation data extracted from the Zetasizer software package for a sample set of data (black). Data were fitted according to a modified version of eq (4) (red). All samples presented were at concentrations of 12 mg/mL.

Dynamic light scattering was used to determine the hydrodynamic radius of the molecules synthesized as part of this study. Measurements were conducted using a commercially available Malvern Zetasizer Nano S90 and the resulting intensity data and autocorrelation function were processed using the software package provided by Malvern for running the instrument. The autocorrelation function is given by

$$g^{(2)}(\tau) = \frac{\langle I(t)I(t+\tau)\rangle}{\langle I(t)\rangle^2}, \tag{3}$$

where $g^{(2)}$ is the correlation coefficient, I is the intensity of the scattered light, t is the time, and τ is the time offset. The Zetasizer software fit this data to a set of exponential decay functions according to the method of cumulants. While it is difficult to replicate this process manually, it is possible to check the results generated by the program by fitting the autocorrelation function to a single exponential decay function

$$g^{(2)}(\tau) = A\exp(-\Gamma\tau) + b, \tag{4}$$

where A and b are fitting parameters and Γ is the decay coefficient. Representative fits using

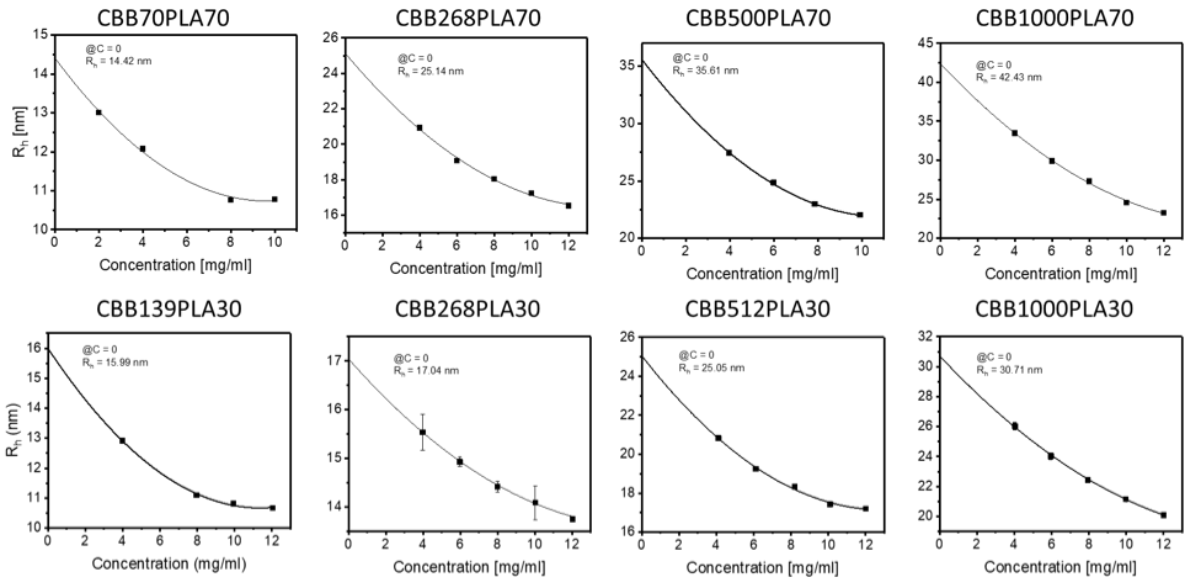

Figure S4: Hydrodynamic radius R_h as a function of concentration for a set example fitted using a second degree power law expansion. For most of the samples, measurements were performed from 4 mg/mL to 12 mg/mL. Zero concentration limits are labeled within each plot.

eq (4) are shown in Figure S3. The decay coefficient is directly related to the diffusivity D and the scattering wave vector q via the equation

$$\Gamma = q^2 D. \tag{5}$$

Based on the conditions under which this measurement is performed, q is calculated to be $0.0303\,\mathrm{nm}^{-1}$. As can be seen from Table S1, the diffusivity calculated from the single exponential fit is very close to that of the method of cumulants. Minor differences in the calculated diffusivity are attributed to the differences in fitting technique as the method of cumulants used by the Zetasizer software also calculates the relative dispersity of the sample. Based on this comparison, it is reasonable to conclude that the results generated by the Zetasizer software package are an accurate representation of the data and can be used to calculate the relative size and dispersity of the bottlebrush polymer.

The hydrodynamic radius is calculated from the diffusivity constant through the appli-

Table S1: Diffusivity calculated by applying a single exponential fit to the autocorrelation function and the diffusivity calculated by the Zetasizer software using the method of cumulants.

Sample	q (nm^{-1})	D_{fit} ($\mu\mathrm{m}^2/\mathrm{s}$)	D_{DLS} ($\mu\mathrm{m}^2/\mathrm{s}$)
CBB268PLA30	0.0303	14.5	15.5
CBB512PLA30	0.0303	17.7	18.1
CBB1000PLA30	0.0303	22.1	22.6

cation of the Stokes-Einstein relation

$$D = \frac{k_B T}{6\pi\eta_s R_h},$$

where k_B is the Boltzmann constant, T is the temperature of the sample during the measurement, and η_s is the viscosity of the solvent.

Both D and R_h are known to vary as a function of the concentration of the sample. As such, it is necessary to remove any concentration dependence from these values by extrapolating D and R_h to the limit of infinite dilution. The relation between R_h and concentration is assumed to be a power series of the form

$$R_h = R_0 + aC + bC^2 + \cdots, \tag{6}$$

where R_0 is the hydrodynamic radius in the limit of infinite dilution, and a and b are series coefficients. Fitting the experimentally determined hydrodynamic radii to eq (6) (truncated after the quadratic term) provides a direct determination of the R_h at zero concentration. Representative fits using this scheme are shown in Figure S4.

2 Simulation method

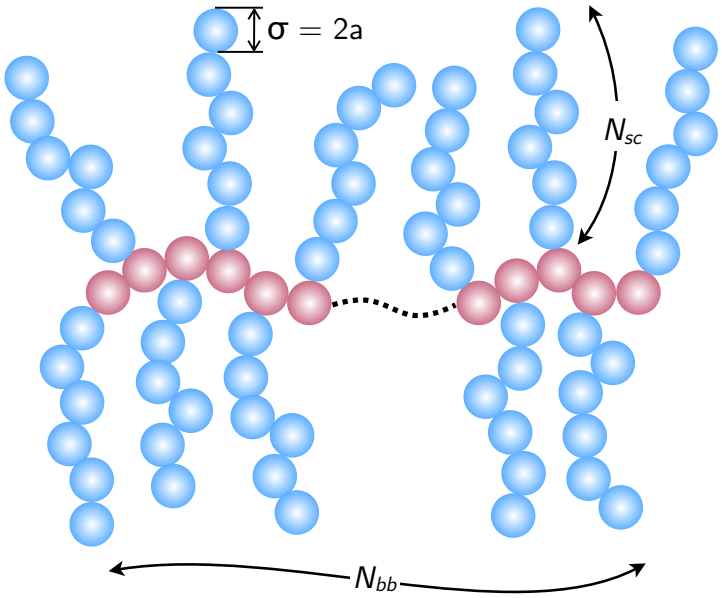

Figure S5: Schematic of our computational model model for a bottlebrush showing the architectural parameters.

Figure S5 shows a schematic for our computational model. The backbone comprises N_{bb} beads, with a side chain of N_{sc} beads attached to each backbone bead. The connectivities between the beads are represented by finitely extensible nonlinear elastic (FENE) springs. The potential for the spring force is:

$$U_s = -\frac{1}{2} k_s r_{\max}^2 \log\left[1 - \left(\frac{r_{ij}}{r_{\max}}\right)^2\right], \quad r_{ij} < r_{\max}. \tag{7}$$

Here, the spring constant is $k_s = 30\varepsilon/\sigma^2$ and the maximum spring extension is $r_{max} = 1.5\sigma$, where r_{ij} is the distance between two connecting beads and σ and ε are the length and energy parameters, respectively.[1]

Excluded volume interaction among the beads is modeled by the truncated and shifted

Lennard-Jones potential:

$$U_{ev} = \begin{cases} 4\varepsilon \left[\left(\frac{\sigma}{r_{ij}}\right)^{12} - \left(\frac{\sigma}{r_{ij}}\right)^{6} \right] - 4\varepsilon \left[\left(\frac{\sigma}{r_{cut}}\right)^{12} - \left(\frac{\sigma}{r_{cut}}\right)^{6} \right], & r_{ij} < r_{cut} \\ 0, \quad \text{otherwise.} \end{cases} \tag{8}$$

For simulations of bottlebrush polymers in an athermal solvent, we set $r_{cut} = 2^{1/6}\sigma$, which makes U_{ev} purely repulsive (also called the Weeks-Chandler-Anderson potential[2]); for the non-athermal case we use $r_{cut} = 2.5\sigma$.

In addition, we also impose a bending penalty on only the backbone beads via the potential:

$$U_b = k_b \left(1 - \cos\theta_{ij}\right), \tag{9}$$

where $k_b = 0.5kT$ and θ_{ij} is defined such that $\cos\theta_{ij} = \hat{\mathbf{u}}_j \cdot \hat{\mathbf{u}}_i$, where $\hat{\mathbf{u}}_i$ and $\hat{\mathbf{u}}_j$ are the unit vectors along consecutive backbone bonds. Note that a bending potential for the backbone beads is not strictly necessary for a generic flexible bottlebrush model, we include it because the experimental system in this study involves bottlebrushes whose backbones (PNB) are significantly stiffer than their side chains (PLA).

The beads are assigned a hydrodynamic radius a and a drag coefficient ζ, representing the friction of a bead. We assume that $a = \sigma/2$ and $\zeta = 6\pi\eta a$, where η is the solvent viscosity.

From the Stokes-Einstein relation, the bead diffusivity is k_BT/ζ and the bead diffusion time is $\tau = \zeta a^2/kT$, where k_B is the Boltzmann constant and T is the absolute temperature. We choose a as the unit of length, k_BT as the unit of energy, and τ as the unit of time. Thus the unit of force is k_BT/a and the unit of diffusivity is k_BT/ζ.

We use a combination of Brownian Dynamics (BD) and Monte Carlo (MC) to evolve the bead positions. The BD position update is via the discretized stochastic differential equation:

$$\mathbf{R}(t+\delta t) = \mathbf{R}(t) - \mathbf{D}(t) \cdot \nabla U(t)\delta t + \sqrt{2\delta t}\ \mathbf{D}^{1/2} \cdot \mathbf{x}, \tag{10}$$

where $\mathbf{R}$ is the column vector of all bead positions, $\mathbf{D}$ is the $3N \times 3N$ diffusivity tensor (N being the total number of beads), $U = U_s + U_{ev} + U_b$ is the total interaction potential, δt is the time step, and $\mathbf{x}$ is a column vector of length $3N$ containing random numbers drawn from a normal distribution $\mathcal{N}(0, 1)$. The third term $\sqrt{2\delta t}\ \mathbf{D}^{1/2} \cdot \mathbf{x}$ represents displacement only due to Brownian motion. The right hand side of the above equation is evaluated using the positions at time t and left hand side gives the bead positions at time $t + \delta t$. Note that eq (10) is in non-dimensionalized form with respect to the units mentioned in the preceding paragraph. Furthermore, for computational expediency we neglect hydrodynamic interaction (HI) between the beads, therefore the diffusivity tensor $\mathbf{D}$ degenerates to the identity matrix.

For the MC part, we use two moves – (i) backbone pivot and (ii) side chain double bridging. The pivot move involves two steps – (a) a backbone bead is chosen randomly, which divides the bottlebrush molecule into two parts and acts as the pivot point; (b) the shorter (in terms of backbone length) part, along with the side chains attached to it, is rotated about the pivot point by an angle chosen from the uniform distribution $\mathcal{U}(0, 2\pi)$. The double bridging move proceeds as follows: (a) two side chains sc_i and sc_j are chosen randomly; (b) bonds connecting beads k and $k+1$ on each chain are broken, where $k \in [1, N_{sc}]$; (c) two new bonds are formed – between bead k of chain sc_i and bead $k + 1$ of chain sc_j, and between bead k of chain sc_j and bead $k + 1$ of chain sc_i. The acceptance of both pivot and double bridging moves are governed by the Metropolis criterion.

A simulation run for a given condition starts with equilibration, using the *slow pushoff* method descibed by Auhl et al[3] (originally in the context of polymer melts), but applied to a single molecule. Six independent trajectories were generated for each case. The time step δt for advancing the beads was $10^{-4}\tau$. A pivot move was performed after every 50 BD time steps and a double bridging sweep was performed after every 11 BD time steps. A sweep involves performing the double-bridging move described earlier repeatedly so as to cover approximately half of the total number of beads. The total duration of all trajectories was 10^8 time steps or more. We checked the approach to equilibrium by monitoring global

size measures of the whole bottlebrush (R_g^2 and R_h) as well as that of the backbone and side chains separately. Sample trajectories are shown in Figure S7. Properties calculated subsequently were averaged over all the trajectories. Errors analysis was performed using by the block-averaging procedure.

2.1 Calculation of R_h and $[\eta]$

The diffusion coefficient we calculated is the so-called Kirkwood diffusivity:[4]

$$D^K = \frac{1}{3N^2} \sum_i \sum_j \mathrm{Tr}\langle \mathbf{D}_{ij} \rangle, \tag{11}$$

where $\mathbf{D}_{ij}$ is the Rotne-Prager-Yamakawa (RPY) tensor,[5,6] which accounts for hydrodynamic interaction between bead i and bead j, N is the total number of beads, and the angle brackets denote average over all conformations. The hydrodynamic radius R_h is then determined using the Stokes-Einstein relation

$$R_h = \frac{k_B T}{6\pi\eta_s D^K}, \tag{12}$$

where η_s is the solvent viscosity. In eq (11), the 3×3 blocks $\mathbf{D}_{ij}$ of the diffusivity tensor are given by

$$\mathbf{D}_{ij} = (1 - \delta_{ij})\, \mathbf{\Omega}_{ij} + \delta_{ij} \mathbf{I}, \qquad i, j = 1, \ldots, N \tag{13}$$

where δ_{ij} is the Kronecker delta, $\mathbf{I}$ is the 3×3 identity matrix, and

$$\mathbf{\Omega}_{ij} = \begin{cases} \dfrac{3a}{4r_{ij}} \left[\left(1 + \dfrac{2a^2}{3r_{ij}^2} \right) \mathbf{I} + \left(1 - \dfrac{2a^2}{r_{ij}^2} \right) \dfrac{\mathbf{r}_{ij}\mathbf{r}_{ij}}{r_{ij}^2} \right], & r_{ij} \geq 2a \\ \left(1 - \dfrac{9r_{ij}}{32a} \right) \mathbf{I} + \left(\dfrac{3r_{ij}}{32a} \right) \dfrac{\mathbf{r}_{ij}\mathbf{r}_{ij}}{r_{ij}^2}, & r_{ij} < 2a. \end{cases} \tag{14}$$

The averaging in eq (11) was performed on equilibrium conformations obtained from a simulation run.

Intrinsic viscosity $[\eta]$ was calculated using the expression derived by Tsuda,[7] which is

based on a non-preaveraged version of Kirkwood theory. A correction factor to Tsuda's theory pointed out by de la Torre and coworkers[8] was incorporated as well. The expression for intrinsic viscosity used here is:[7–9]

$$[\eta] = \frac{5}{2}\frac{N_A V_1}{M_1} + \frac{N_A}{6M\eta_s}\left\langle \frac{\zeta \sum_i R_i^2}{1 + \dfrac{\zeta Q}{8\pi\eta_s \sum_i R_i^2}} \right\rangle, \tag{15}$$

where $\zeta = 3\pi\eta_s\sigma$ is the friction coefficient of a bead, N_A is the Avogadro number, $V_1 = \pi\sigma^3/6$ is the volume of a bead, M_1 is the molar mass of a bead, and

$$Q = \sum_l \sum_s{}' \left[\frac{\mathbf{R}_l \cdot \mathbf{R}_s}{R_{ls}} + \frac{1}{10R_{ls}^3}\left\{ 4\left(R_l^2 + R_s^2\right)\mathbf{R}_l \cdot \mathbf{R}_s - R_l^2 R_s^2 - 7\left(\mathbf{R}_l \cdot \mathbf{R}_s\right)^2 \right\} \right],$$

where $\mathbf{R}_i$ is the position vector of bead i with respect to the molecule center-of-mass, $R_i = \|\mathbf{R}_i\|$, and $R_{ij} = \|\mathbf{R}_i - \mathbf{R}_j\|$. In eq (15), the first term in the left hand side is a correction term introduced to account for the limiting case of a single bead,[8] the expression inside the angle brackets was derived by Tsuda[7] for rigid molecules based a non-preaveraged version of Kirkwood theory, and the angle brackets were put in by de la Torre et al[9] to account for conformational fluctuations in flexible molecules. Substituting the expressions for ζ, V_1, and $M_1 = M/N$, we rewrite eq (15) in a more amenable form:

$$[\eta] = \left(\frac{5\pi N_A}{12}\right)\frac{N\sigma^3}{M} + \frac{\pi N_A \sigma}{2M}\left\langle \frac{\sum_i R_i^2}{1 + \left(\dfrac{3\sigma}{8}\right)\dfrac{Q}{\sum_i R_i^2}} \right\rangle. \tag{16}$$

The average denoted by the angle brackets in eq (16) was performed on the conformations obtained from simulations.

For simulations on linear polymers using the above method, we find that the mass scaling exponents calclated for R_h and $[\eta]$ agree very well with those predicted based on Zimm dynamics,[10] as shown in Figure S6.

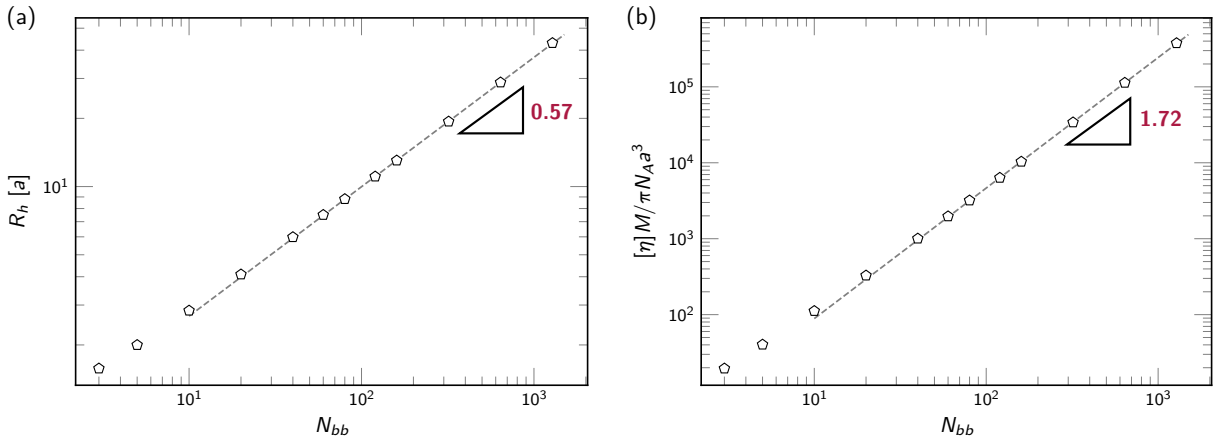

Figure S6: (a) Hydrodynamic radius (R_h) and (b) rescaled intrinsic viscosity ($[\eta]$) of linear polymers determined from simulations using the method described in 2.1. The scaling exponents shown agrees well with the predictions based on Zimm dynamics in dilute solution.

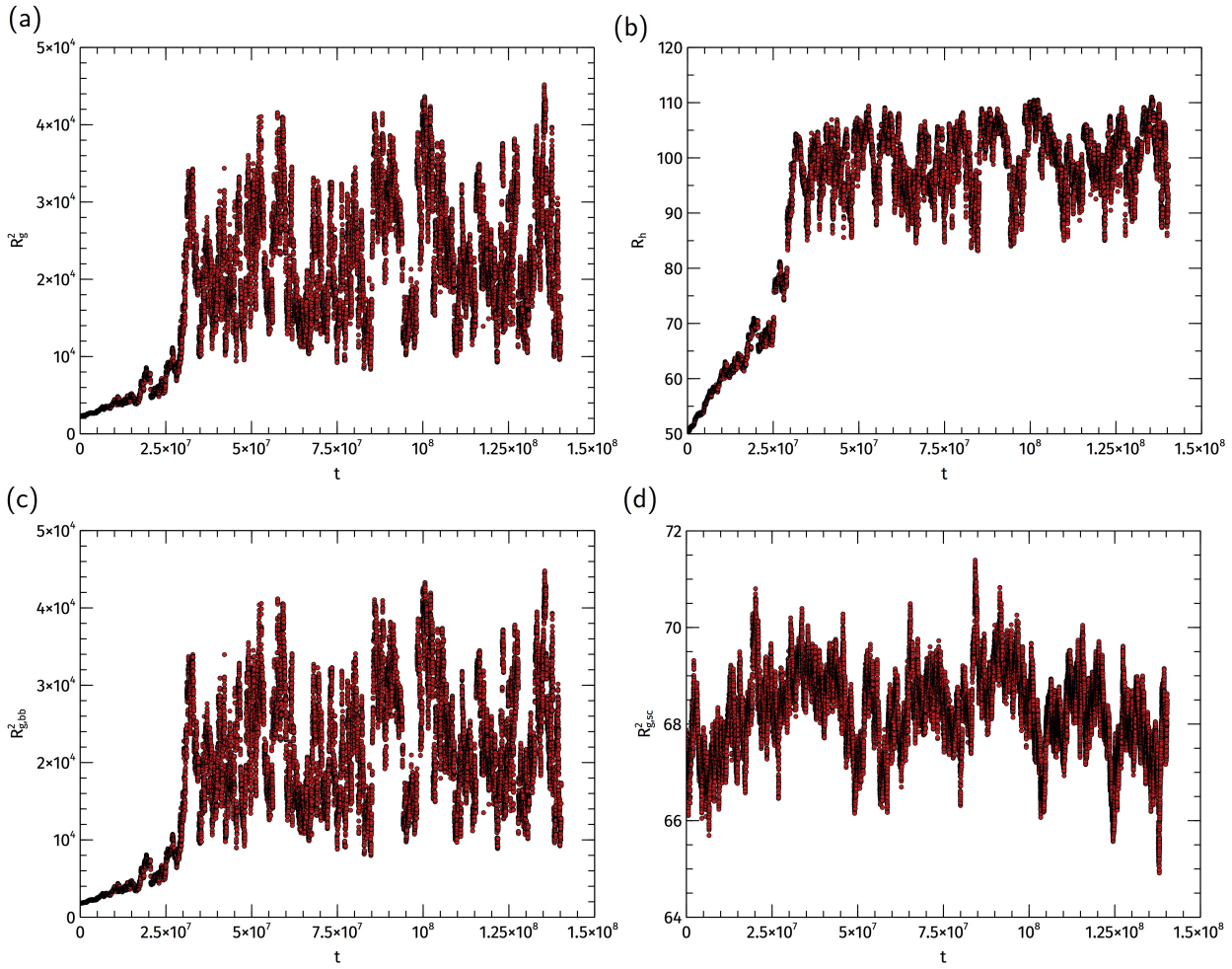

Figure S7: Size measures showing approach to equilibrium for $N_{bb} = 640$ and $N_{sc} = 32$: (a) Mean-squared radius of gyration (R_g^2) of the whole bottlebrush, (b) Hydrodynamic radius R_h of the whole bottlebrush, (c) Mean-squared radius of gyration of the backbone ($R_{g,bb}^2$), and (d) Mean-squared radius of gyration of the side chains ($R_{g,sc}^2$). Note that the data shown is after removal of all force-capping. Length and time are in simulation units.

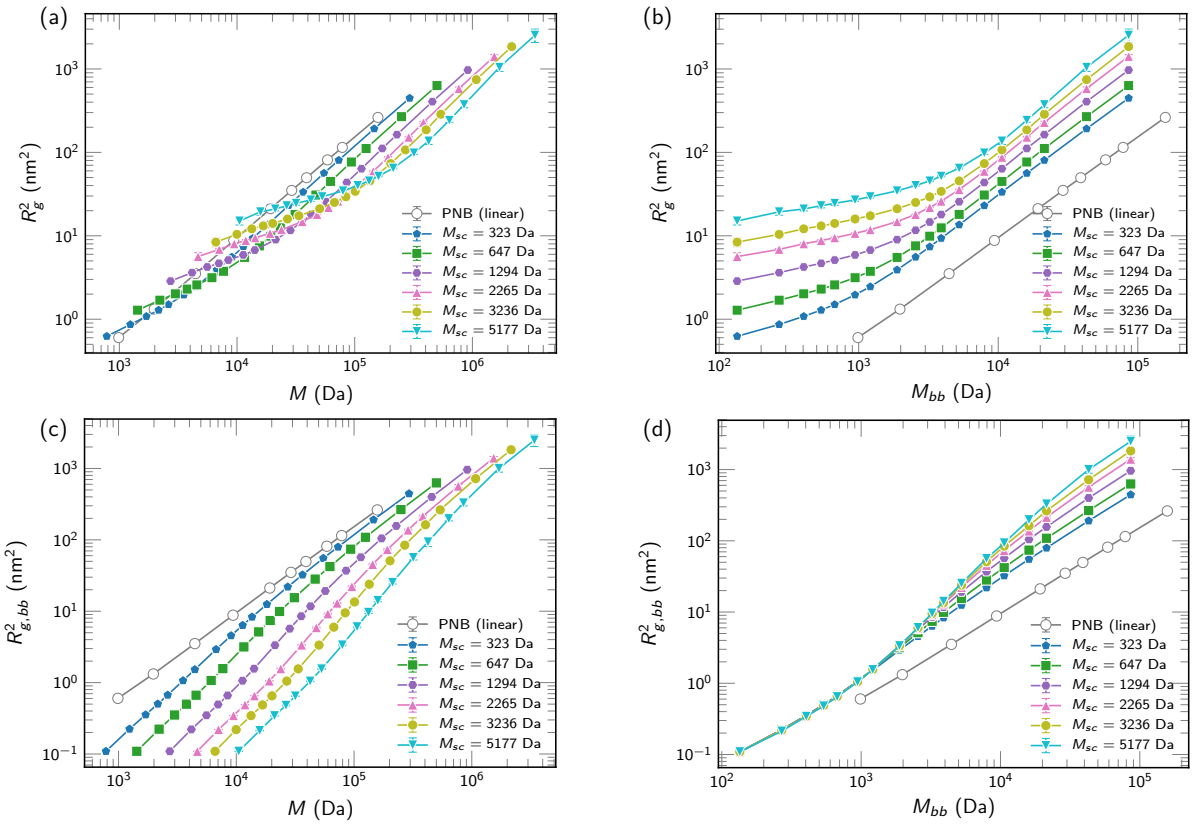

Figure S8: Mean-squared radius of gyration (R_g^2) as a function of total molecular weight M (a) and backbone molecular weight (b) for different side chain molecular weights (M_{sc}). Mean-squared radius of gyration of the backbone ($R_{g,bb}^2$) as a function of total molecular weight M (c) and backbone molecular weight (d) for different side chain molecular weights (M_{sc}). Solid lines are intended to guide the eye.

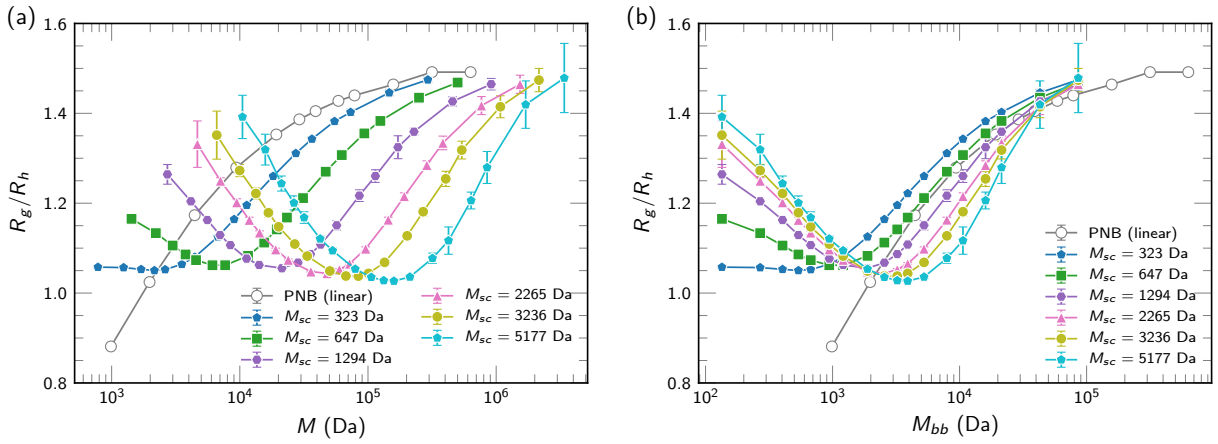

Figure S9: Ratio of radius of gyration to hydrodynamic radius *vs.* molecular weight of the entire bottlebrush (a) and backbone molecular weight (b) for different side chain molecular weights (M_{sc}). Solid lines are intended to guide the eye.

References

(1) Kremer, K.; Grest, G. S. Dynamics of entangled linear polymer melts: A molecular-dynamics simulation. *J. Chem. Phys.* **1990**, *92*, 5057–5086.

(2) Weeks, J. D.; Chandler, D.; Andersen, H. C. Role of repulsive forces in determining the equilibrium structure of simple liquids. *J. Chem. Phys.* **1971**, *54*, 5237–5247.

(3) Auhl, R.; Everaers, R.; Grest, G. S.; Kremer, K.; Plimpton, S. J. Equilibration of long chain polymer melts in computer simulations. *J. Chem. Phys.* **2003**, *119*, 12718–12728.

(4) Dünweg, B.; Reith, D.; Steinhauser, M.; Kremer, K. Corrections to scaling in the hydrodynamic properties of dilute polymer solutions. *J. Chem. Phys.* **2002**, *117*, 914–924.

(5) Rotne, J.; Prager, S. Variational treatment of hydrodynamic interaction in polymers. *J. Chem. Phys.* **1969**, *50*, 4831–4837.

(6) Yamakawa, H. Transport properties of polymer chains in dilute solution: Hydrodynamic interaction. *J. Chem. Phys.* **1970**, *53*, 436–443.

(7) Tsuda, K. Intrinsic viscosity of rigid complex molecules. *Rheol. Acta* **1970**, *9*, 509–516.

(8) Carrasco, B.; de la Torre, J. G. Hydrodynamic properties of rigid particles: Comparison of different modeling and computational procedures. *Biophys. J.* **1999**, *76*, 3044–3057.

(9) de la Torre, J. G.; Martinez, M. C. L.; Tirado, M. M. Monte Carlo study of hydrodynamic properties of flexible linear chains: Analysis of several approximate methods. *Macromolecules* **1984**, *17*, 2715–2722.

(10) Rubinstein, M.; Colby, R. *Polymer physics*; Oxford University Press, N. Y., 2003.